Large-scale influences on secondary eyewall size

Xiaqiong Zhou[1] and Bin Wang[2]

Received 26 March 2013; revised 12 June 2013; accepted 25 June 2013; published 1 October 2013.

[1] Secondary eyewalls are frequently observed in intense tropical cyclones (TCs). The separation distance between the primary eyewall and the secondary eyewall can vary from 10 to more than 100 km. The size of the secondary eyewall is a key factor determining the horizontal scale of the destructive winds and heavy rainfall in these TCs. Previous work suggested that the internal dynamic and thermodynamic structure of the TC affects the radial location of secondary eyewall formation. The potential impact of the large-scale environment is examined by using the National Centers for Environmental Prediction-National Center for Atmospheric Research reanalysis and best track data sets in this study. It is found that large secondary eyewalls tend to form in weak storms at relatively high latitudes and in environments with high relative humidity, low sea-level pressure, and high low-level vorticity. The performance of a statistical-dynamical model to predict the size of secondary eyewalls is evaluated, and the physical interpretation of the selected predictors is also provided.

Citation: Zhou, X., and B. Wang (2013), Large-scale influences on secondary eyewall size, *J. Geophys. Res. Atmos.*, *118*, 11,088–11,097, doi:10.1002/jgrd.50605.

1. Introduction

[2] Secondary eyewalls often occur in intense tropical cyclones (TCs), generally with maximum sustained wind speeds greater than $60\,m\,s^{-1}$ [*Fortner*, 1958; *Willoughby et al*., 1982; *Black and Willoughby*, 1992; *Hawkins et al*., 2006; *Sitkowski et al*., 2011]. A secondary wind maximum is often collocated with the secondary eyewall, analogous to the collocation of the peak winds and convection in the primary eyewall [*Samsury and Zipser*, 1995]. Between the two concentric eyewalls is a "moat," a nearly convection-free annulus. TCs can experience dramatic changes not only in intensity but also in size as a result of secondary eyewall formation [*Maclay et al*., 2008]. The storm intensity weakens due to the gradual erosion of the inner eyewall. The development of the convective secondary eyewall leads to a dramatic broadening of the damaging winds, meaning that the size of the secondary eyewall affects the extent of damaging wind, heavy rainfall, and sometimes the storm surge associated with TCs. The secondary eyewall size also affects the time required for the eyewall replacement and associated intensity change [*Zhou and Wang*, 2011]. Consistent with *Shapiro and Willoughby*'s [1982] time scale analysis of the evolution of a convective ring, *Zhou and Wang* [2011] found that a relatively small outer eyewall often replaces the inner eyewall quickly. They also suggested that a storm with a large secondary eyewall tends to experience large intensity fluctuations since the outer eyewall has to establish a much larger warm core that includes the previous eye and moat.

[3] Over past decades, a number of hypotheses have been proposed to explain secondary eyewall formation [*Willoughby et al*., 1984; *Kuo et al*., 2004, 2008; *Huang et al*., 2012; *Fang and Zhang*, 2012; *Rozoff et al*., 2012; *Wang et al*., 2013; *Abarca and Montgomery*, 2013; *Kepert*, 2013]. An important consideration involves determination of the secondary eyewall's radial location or the separation distance between concentric eyewalls. Some researchers suggested that the radial location of the secondary eyewall is related to the TCs' dynamic/thermodynamic structure. *Montgomery and Kallenbach* [1997] hypothesized that outer eyewalls form at the stagnation radius of outward propagating vortex Rossby waves where they can accelerate the mean tangential flow through eddy momentum flux convergence. The radial location of secondary eyewalls is also an issue of the moat width. The tendency for convection to be suppressed in the moat is generally attributed to mesoscale subsidence between two regions of strong upward motion [*Dodge et al*., 1999; *Houze et al*., 2006, 2007]. *Rozoff et al*. [2006] proposed that weak-echo moats could be a result of strong horizontal straining. *Kuo et al*. [2009] found that the width of the filamentation zone explains about 40% of the variance of the observed moat width in 19 cases with TC intensity greater than 130 kT. *Terwey and Montgomery* [2008] proposed that a region with a weak negative radial potential vorticity gradient associated with the primary swirling flow, named the "β-skirt," is required for the formation of a secondary eyewall. Deep convection within the β-skirt acts as a source of perturbation eddy kinetic energy and vorticity. A finite-amplitude lower tropospheric cyclonic jet outside the primary eyewall with a jet width on the order of the local

[1]IMSG at NCEP, NWS, NOAA, College Park, Maryland, USA.
[2]International Pacific Research Center and Department of Meteorology School of Ocean and Earth Science and Technology, University of Hawai'i at Mānoa, Honolulu, Hawaii, USA.

Corresponding author: X. Zhou, IMSG at NCEP, NWS, NOAA, 5830 University Research Ct., College Park, MD 20740, USA. (xiaqiong.zhou@noaa.gov)

©2013. American Geophysical Union. All Rights Reserved.
2169-897X/13/10.1002/jgrd.50605

effective β scale might be initiated by the axisymmetrization of convectively generated vorticity anomalies. Thereafter, a secondary eyewall forms through the wind-induced surface heat exchange (WISHE) mechanism. *Zhou and Wang* [2011] found that ice-phase microphysics may affect the radial location of secondary eyewalls. Their numerical sensitivity experiments show that the secondary eyewall forms at an increased radius with enhanced ice concentrations.

[4] Some researchers have argued that the secondary eyewall formation requires external forcing. *Nong and Emanuel* [2003] hypothesized that the interaction with baroclinic eddies, topography, or sea surface temperature (SST) variations are likely the types of perturbations needed for secondary eyewall formation through WISHE. A naïve Bayesian probabilistic model for the prediction of imminent secondary eyewall formation has been developed by *Kossin and Sitkowski* [2009] based upon large-scale environmental conditions and features observed from geostationary satellite. The model provides a conditional probability of two classes, the occurrence or absence of secondary eyewall formation. In independent testing, the algorithm performs skillfully against a defined climatology. It confirms that environmental conditions surrounding TCs could play an essential role in secondary eyewall formation.

[5] The potential effect of TC-ambient conditions' influence on the secondary eyewall size has not been studied so far. In this study, the climatology associated with the radial location of secondary eyewalls and the local environmental conditions prior to and at the time when secondary eyewalls are detected are studied. Section 2 describes the data used and the details of computing the environmental parameters. Section 3 outlines the general information of secondary eyewall events, especially related to their radial location. In section 4, an empirical model is derived, and associated physical interpretation is presented in section 5. Finally, a summary and discussion are given in section 6.

2. Data and Methodology

[6] The secondary eyewall cases used in this study are the same as in *Kuo et al.*'s [2009] work except for a longer period (from 1997 to 2009). There are a total of 69 secondary eyewall events in 62 typhoons during the 13 year period. The secondary eyewall events are defined based on passive Special Sensor Microwave/Imager 85 GHz horizontal polarized orbital images and passive Tropical Rainfall Measuring Mission (TRMM) microwave imager data from the polar-orbiting TRMM satellite [*Kummerow et al*., 1998] on the Naval Research Laboratory website [*Kuo et al*., 2009]. The microwave data are used to identify secondary eyewall structure and the width of moat between concentric eyewalls. A secondary eyewall is identified when deep convection with a total blackbody temperature, Tbb, approximately 230 K is covering at least two thirds of a circle. The moat is the high brightness temperature ($>$ 230 K) region between the eyewalls. The interest of this study is the variation of moat width, the separation distance between concentric eyewalls. It is determined by averaging the measured values from eight radial arms. More details about the definition of a secondary eyewall and moat size can be found in *Kuo et al.*'s [2009] paper. The inner eyewall exists prior to the formation of a secondary eyewall. It is one of the important properties of an intense storm when it is still a single-eyewall storm. *Kuo et al*. [2009] found that there is no significant correlation between the moat width and the size of the inner eyewall. To simplify, the variation of moat width, instead of the radius of the secondary eyewall from the storm center, is used to describe the variation of the secondary eyewall size. The variation of the inner eyewall size is excluded in this study.

[7] The other data sets used include the best track data set from the Joint Typhoon Warning Center (JTWC; http://jtwccdn.appspot.com/NOOC/nmfc-ph/RSS/jtwc/best_tracks/) and National Centers for Environmental Prediction-National Center for Atmospheric Research (NCEP/NCAR, Version 2) [*Kalnay et al*., 1996] four-time daily reanalysis data set with 2.5° latitude-longitude resolution. The JTWC best track data set provides typhoon intensity and location. The NCEP/NCAR reanalysis data are used to compute environmental quantities in the secondary eyewall cases. We account for the irregular time of secondary eyewall events based on satellite observations with regular 6 h resolution of the JTWC best track data and NCEP/NCAR reanalysis data by matching the time closest to the secondary eyewall event. To produce a better estimate of the TC's environment, a Tukey window spatial low pass filter [*Hendricks et al*., 2010] is used to minimize the effect of TC circulation signature on environmental variables. The variability on horizontal scales smaller than 7.5° latitude/longitude is filtered.

[8] The Shapiro-Wilk test [*Shapiro and Wilk*, 1965] is used to test whether the moat size and potential factors are normally distributed. The relationship between the size of the secondary eyewall and a set of environmental and TC parameters is examined by using the Pearson's correlation coefficient. Two groups of secondary eyewall cases with extremely wide moat and narrow moat widths are selected, and a Student's t test is used to compare the means of the environmental and TC factors in these two groups. The stepwise regression procedure is used to identify the most important factors influencing secondary eyewall size. Boxplots are used to identify outliers and indicate the median, skewness, and degree of spread in the data. The Kruskal-Wallis median test [*Kruskal and Wallis*, 1952], a nonparametric test used to compare the median of two or more groups having skewed distributions with outliers, is also used.

3. Climatology

[9] The climatology of secondary eyewall events from 1997 to 2006 over the western North Pacific (WNP), especially its relationship with storm intensity change compared with the nonconcentric cases, has been studied by *Kuo et al.* [2009]. We primarily focus on the climatological features that are related to the moat width.

[10] Almost all secondary eyewall events (67 of 69) occur in major typhoons (Saffir-Simpson categories 3 to 5). The probability of secondary eyewall occurrence increases with storm maximum intensity (Table 1): Approximately 24% of category 3, 48% of category 4, and 74% of category 5 typhoons possess secondary eyewall structures in their life span. However, secondary eyewalls are not necessarily identified at the storm peak intensity. On average, the detection of secondary eyewall microwave imagery lags the time of the maximum intensity by

Table 1. The Number of Categories 1 to 5 Typhoons, the Number of Typhoons With at Least One Secondary Eyewall Event, the Frequency of Secondary Eyewall Events, and the Percentage of Typhoons With at Least One Secondary Eyewall Event as a Function of the Typhoons' Maximum Intensity (Grouped by Saffir-Simpson Category)

	Cat.1	Cat. 2	Cat.3	Cat.4	Cat.5
WNP TC		32	25	58	35
Secondary eyewall TC	0	2	6	28	26
Secondary eyewall events	0	2	6	29	32
Percentage		6%	24%	48%	74%

26 h. Less than one third of secondary eyewalls (23 of 69) are detected in a 6 h window of the peak intensity. Only a small portion (10%) occurs before the peak intensity window. Of the cases that secondary eyewalls form 6 h or more after the time of the maximum intensity (41), more than half (26) lagged the peak intensity by more than 24 h.

[11] Seven typhoons undergo double secondary eyewall events in their life spans. The multiple secondary eyewall events are preferably associated with very intense storms. Six of them are category 5 typhoons on the Saffir-Simpson scale, while the weakest one also reaches category 4 strength. As the secondary eyewall replacement cycles are repeated, the secondary eyewall usually forms at a larger radius. The only exception is Typhoon Nita (2005), for which the width of the moat is slightly narrower in the second cycle when observed 3 days later.

[12] Figure 1a depicts the distribution of secondary eyewall events in terms of the TC intensity when secondary eyewalls are identified. The secondary eyewall events with major typhoon intensity at the time of the detection account for 84% (58 events). The secondary eyewalls forming in categories 1 and 2 stages only account for 16% (11 cases) of all cases. The average intensity is 119.7 kT. The mean width of moats is 33.7 km with a 21.3 km standard deviation. A few TCs developed the outer eyewalls at an extremely large radius (Figure 2). For example, the width of the moat between the concentric eyewalls in Typhoon Winnie (1997) reaches 150 km. This storm did not experience contraction of the outer eyewall and subsequent dissipation of the inner one. The double eyewall structure was evident until it reached the shoreline. In contrast, the outer eyewalls in Typhoons Sinlaku (2002), Kujira (2003), and Sudal (2004) are close to the inner one with a distance of less than 20 km (Figure 2).

[13] The mean width of the moat decreases with increasing intensity from categories 2 to 5 typhoons (Figure 1a). The moat width of category 1 storms is not representative for this category due to small sample size. The mean width of the moats in category 2 storms is 57.7 km, and it decreases to 37.8 km in category 3, 30 km in category 4, and 24.9 km in category 5. The width median has a similar tendency (Figure 1b). A Kruskal-Wallis median test is applied to compare the median moat width in different categories from categories 2 to 5. The test shows that the differences of the width median are significant at the 99% confidence level for these categories. In addition, the moat widths are positively skewed. Most of the secondary eyewalls tend to form at smaller radius. It is possible that a large secondary eyewall is more vulnerable to hostile environment and more difficult to form than a small one. The variation of moat size is not normally distributed, but the logarithm of moat size passes the Shapiro-Wilk normality test. Another interesting feature is that the variation of moat width decreases with storm intensity. Variations of the moat widths in categories 2 and 3 are larger than in category 5 storms.

[14] Figure 3 presents the seasonal variation of secondary eyewall events. Secondary eyewalls were observed from April to December, primarily between June and October. The seasonal variations of secondary eyewall events are only discussed in the storm peak season (from June to October) given the small frequency in other months. The mean latitude of secondary eyewall formation shifts northward from June and back to the equatorial side in October, which is consistent with the mean seasonal migration of TC activity [*Wang and Zhou*, 2008]. The mean moat width is inversely related to the intensity in the seasonal evolution. During the TC peak season (June to October), the minimum mean intensity of secondary eyewall events appear in August (110 kT) with the mean moat width of 40 km. The moat width decreases to 30 km in October as the mean intensity increases to 130 kT.

[15] The yearly total number of secondary eyewall events ranges from 2 to 10 (Figure 4a). Its interannual variation is highly correlated with the frequency of the major typhoons occurrence with intensity > 94 kT ($r = 0.81$) in 6-hourly intervals. This further confirms that the secondary eyewalls are a common feature of intense storms.

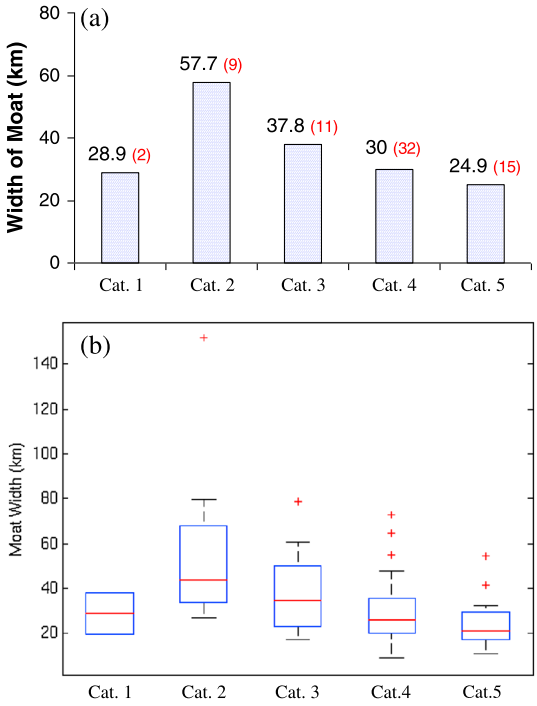

Figure 1. (a) The mean width of moats and the frequency of secondary eyewall events (number in parentheses) as a function of current intensity (grouped by Saffir-Simpson category). (b) The box-and-whisker diagram of the moat width in TCs with intensity from categories 1 to 5. The bottom and top of the box are lower and upper quartile, and the band near the middle is the median. The ends of the whiskers represent 1.5 times of the lower and upper quartile.

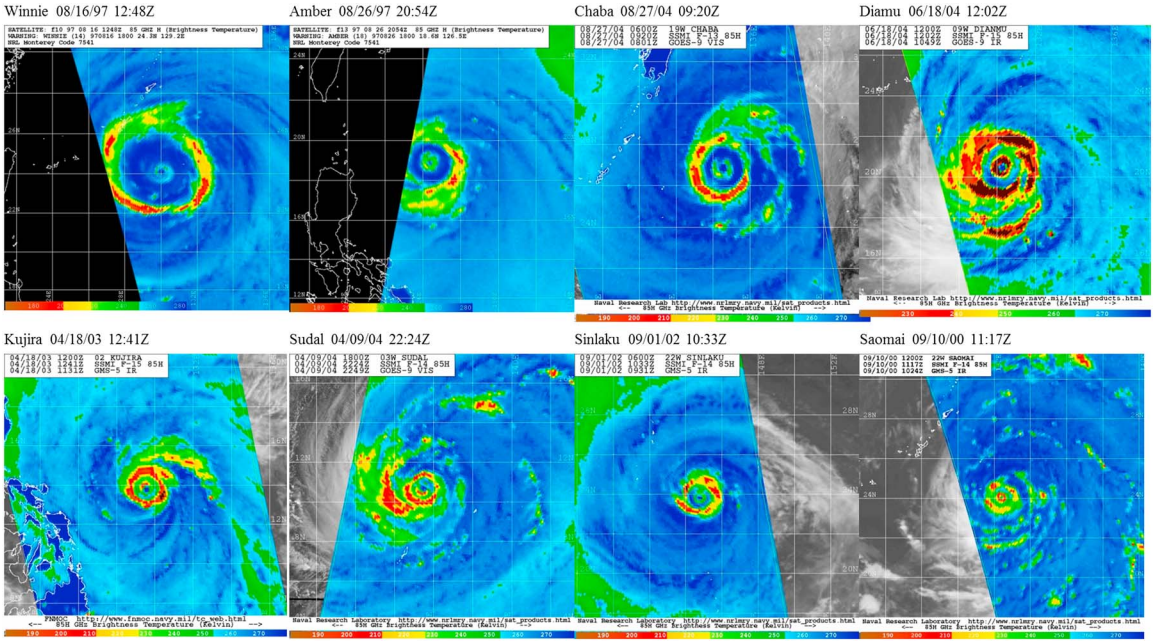

Figure 2. Microwave images of eight secondary eyewall cases with secondary eyewall structure. Storm names, dates, and times are given in each individual image panel.

4. Potential Factors and Their Connections to Secondary Eyewall Size

[16] In this section, the secondary eyewall events close to land are excluded in order to avoid the influence of land. A total of 54 cases are available for analysis. Potential factors that may influence the secondary eyewall size include environmental and TC parameters. They are calculated prior to the secondary eyewall formation up to 48 h with a 6 h interval.

4.1. Potential Predictors

[17] The relationship between the secondary eyewall size and the potential factors that are used for prediction of the intensity change, such as the Statistical Typhoon Intensity Prediction Scheme (STIPS) for the WNP [*Knaff et al.*, 2005] and the Statistical Hurricane Intensity Prediction Scheme (SHIPS) for the Atlantic and East Pacific basins [*DeMaria et al.*, 2005], is investigated. *Kossin and Sitkowski* [2009] also use SHIPS data to study the environment surrounding tropical cyclones favorable for secondary eyewall formation in the North Atlantic and central and eastern North Pacific, but their interest is the relationship between these environmental factors with the possibility of secondary eyewall formation. The factors that are associated with not only secondary eyewall formation but also storm size documented in previous literature are considered since secondary eyewall formation involves significant changes in storm size [*Maclay et al.*, 2008]. The factors affecting storm size probably also play a role in modulating the size of the secondary eyewall.

[18] There are two types of factors that are derived along the TC track (Table 2): (1) those related to TC intensity and location, named "static predictors" in STIPS/SHIPS, and (2) those related to time-dependent environmental conditions. The static predictors include TC intensity estimated by surface maximum wind speed (VMX), 12 and 24 h intensity change (DVMX12 and DVMX24), and TC's forward speed (SPD). Many previous studies have found that the high-latitude storms have stronger outer-core winds or larger size [*Yamasaki*, 1968; *Merrill*, 1984; *Weatherford and Gray*, 1988a, 1988b]. Thus, the latitude of the TC center (LAT) is included in the statistical predictor pool.

[19] The environmental factors are azimuthally averaged within the 300 to 600 km annulus from the TC center except for those noted below and in Table 2. These environmental factors can also be divided into two categories. One category of environmental factors is related to large-scale wind fields, named dynamic factors. At 200 hPa, the environmental zonal wind, the divergence, and the relative eddy flux convergence

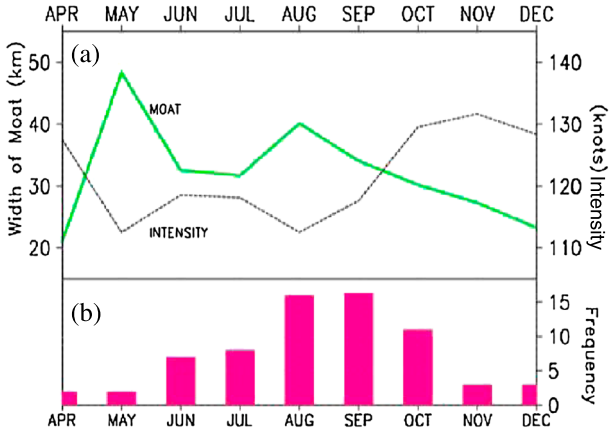

Figure 3. (a) The average width of moats and the average intensity and (b) the frequency of secondary eyewall events by month.

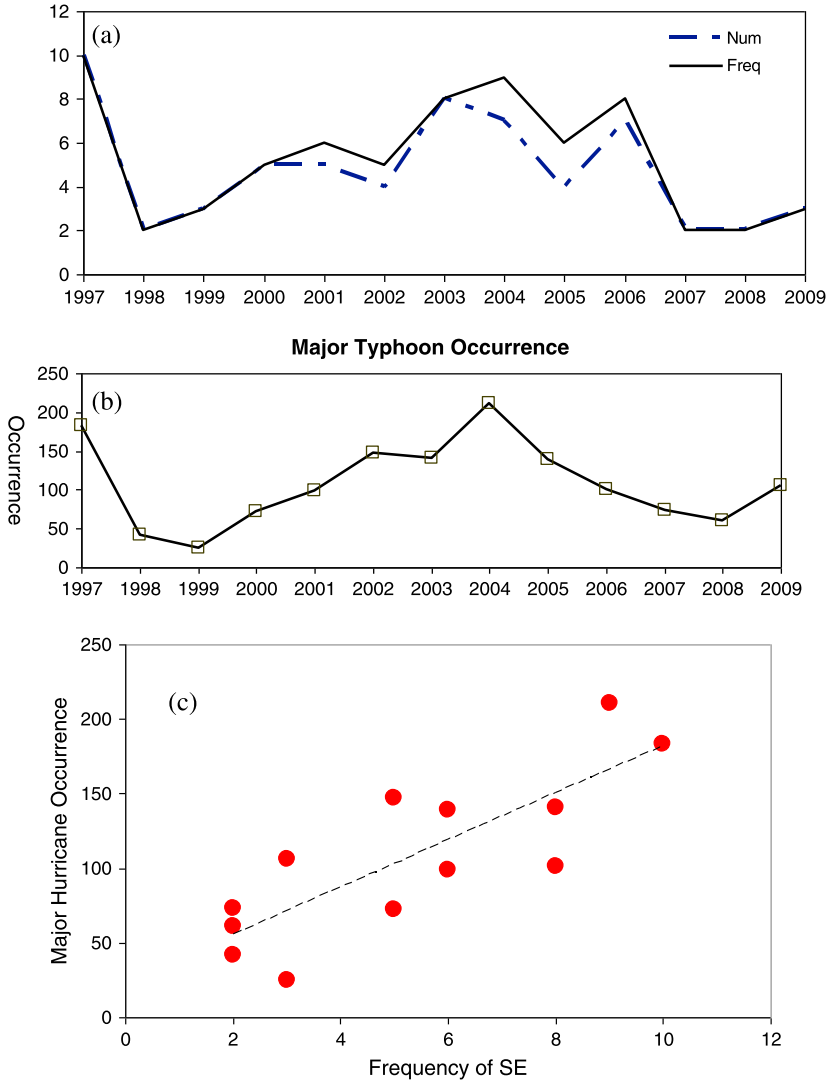

Figure 4. (a) The time series of the secondary eyewall frequency (solid line) and the number of TCs with at least one secondary eyewall event (dashed line) and (b) the occurrence of major typhoon over the WNP. (c) Scatter diagram showing the close relationship between secondary eyewall frequency and major typhoon occurrence. The frequency of the TC occurrence is counted for each 6 h interval from best track data.

(REFC) are examined. The divergence is averaged over a slightly larger area (<1000 km), and the REFC is calculated within 600 km following equation (2) in *Knaff et al*. [2005]. At 850 hPa, the area-averaged symmetric tangential winds (TWAC) and vorticity (VOR850) are calculated as potential factors. The magnitude of the vector wind difference between 200 and 850 hPa, as well as the difference between 500 and 850 hPa, is employed to represent the environmental vertical wind shear. The zonal wind components of the shear in these layers are also examined. Azimuthally averaged environmental sea-level pressure (PENC) is grouped into the dynamic category due to its possible connection with the storm winds in the outer region. TCs are well approximated by gradient wind balance in the outer region, and thus, the environmental pressure could affect the storm's outer wind field [*Willoughby*, 1990; *Willoughby and Rahn*, 2004].

[20] Another category of environmental factors that could affect convective activity in the storm outer region is named thermodynamic factors. Humidity of the lower to middle level tropospheric air is the dominant factor affecting convection [*Houze*, 1993]. The entrainment of environmental unsaturated air will reduce the buoyancy of convective cells. The variations of the low-level and upper level environmental relative humidity are calculated at 850 to 700 hPa and 500 to 300 hPa. Among the environmental quantities, relatively large uncertainties might exist in relative humidity [*Trenberth and Guillemot*, 1998]. However, these uncertainties in the moisture variables should not affect the results considerably since only the large-scale patterns and variations are examined.

[21] The maximum potential intensity (MPI) is a conceptualized upper limit on the intensity of a TC [*Emanuel*, 1986]. As an essential variable in the SHIPS/STIPS model to predict TC intensity change, it can be estimated from the large-scale thermodynamic environment by using NCEP/NCAR oceanic skin temperature, surface pressure, and air temperature and relative humidity (RH) vertical profiles according to the method developed by *Emanuel* [1986].

Table 2. Potential Synoptic Predictors Available for Inclusion Into the Prediction of the Radial Location of Secondary Eyewalls

Factor	Description
	Static factors
VMX	Current intensity (kT)
LAT	Current central latitude
DVMX24	24 h intensity change
DVMX 12	12 h intensity change
SPD	Storm translational speed
	Dynamic factors
200 hPa	
U200	200 hPa zonal wind (300–600 km)
DIV200	200 hPa divergence (<1000 km)
REFC	200 hPa relative eddy flux convergence (<600 km)
850 hPa	
VOR850	850 hPa vorticity (<1000 km)
TWAC	850 hPa symmetric tangential wind (300–600 km)
Wind Shear	
SHRD	500–850 hPa horizontal wind vertical shear (300–600 km)
SHRS	200–850 hPa zonal wind vertical shear (300–600 km)
USHRD	500–850 hPa zonal wind vertical shear (300–600 km)
USHRS	200–850 hPa horizontal wind vertical shear (300–600 km)
PENC	Azimuthally averaged sea-level pressure at (300–600 km)
	Thermodynamic factors
RHHI	500–300 hPa relative humidity (300–600 km)
RHLO	850–700 hPa relative humidity (300–600 km)
MPI	Maximum potential intensity (300–600 km)
T200	200 hPa temperature (300–600 km)
CAPE	Convective available potential energy (300–600 km)
SST	Sea surface temperature (300–600 km)

[22] The temperature surrounding the TC at the 200 hPa level is considered as a forecasting factor for TC intensification [*DeMaria et al*., 2005; *Knaff et al*., 2005] as TCs are fueled by deep convection. Low temperatures at 200 hPa are favorable for TC intensification with its contributions linked to the increasing potential convective instability [*Knaff et al*., 2005] and MPI [*Emanuel*, 1986].

[23] The environmental convective available potential energy (CAPE) is examined by using the temperature and RH in the NCEP reanalysis since previous studies have shown that sufficient CAPE is required for the development of convection in the outer region prior to secondary eyewall formation [*Terwey and Montgomery*, 2008]. Despite coarse resolution of the reanalyses data, a previous study has shown that the large-scale CAPE calculated from reanalyses data is still valuable in identifying extreme convective events [*Cheung*, 2004]. The CAPE from the global reanalyses is examined as a large-scale condition for convection surrounding TCs.

[24] The composite, correlation, and multiple stepwise regression analyses are performed to study major factors affecting moat width. Logarithmically transformed moat size and those factors that pass the Shapiro-Wilk test are used so that the statistical significance can be assessed by using the *t* test and the *F* test, in which normal distribution of the data is assumed. Some environmental factors are related to each other. For example, the estimate of MPI depends on RH and temperature profiles, and it is expected that MPI is also correlated with the storm intensity. The stepwise regression allows the selection of multiple independent variables, as few explanatory variables as possible, to ensure an easy-to-interpret model.

4.2. Composite and Correlation Analyses

[25] The composite analysis is conducted by comparing the potential factors in two groups of secondary eyewall TCs with wide and narrow moats. The cases in these two groups with the deviation of the logarithm of moat width from the mean more than 1.5 standard deviation are selected. The group with wide moats includes 16 cases with an average width of 66.1 km, and the group with narrow moats has 12 cases with an average moat width of 17.8 km (Table 3). A Student's *t* test is used to compare the means of the two groups. The differences are significant at the 95% confidence level listed.

[26] The mean intensity of the storms with narrow moats (127.5 kT) is stronger than those with wide moats (112.5 kT). There is a significantly different tendency of intensity change prior to formation between these two groups although their subsequent weakening rates are similar (Figure 5). The storms with narrow moats experience rapid intensification prior to the formation and reach peak intensity when the secondary eyewalls are observed. By contrast, the storms with wide moats persist at high intensity, higher than those with narrow moats in the early stage, but become weaker from 24 h prior to the secondary eyewall formation. The intensity tendencies in these two groups are also examined according to the 24 h intensity change following *Kuo et al*.'s [2009] classification. The results show that intensification prior to formation is more frequently observed in storms with narrow moat (81%) than those with wide moat (58%).

[27] Significant differences between these two groups are also identified in the latitude of location and some environmental variables. The storms with wide moats are generally located at higher latitude (22.4°N) than those with narrow moats (18.7°N). In addition, the storms with wide moats have higher relative humidity in the lower and upper troposphere, lower sea-level pressure, warmer upper level temperatures, and stronger low-level symmetric winds than its counterpart.

[28] Similar connections between secondary eyewall size and these parameters can be identified with correlation analyses (Table 3). The time-lead correlations of the potential factors with the secondary eyewall moat width are further calculated to examine the potential predictability. The time of secondary eyewall formation is used as the reference time. The correlations with T200 and PENC remain significant

Table 3. Composite Mean Values for the Two Groups of TCs: TCs With Wide Moats and Narrow Moats[a]

	MOAT (km)	VMX (kT)	LAT (°N)	MPI (kT)	RHHI (%)	RHLO (%)	TWAC ($m\,s^{-1}$)	PENC (hPa)	T200 (°C)
Wide moat ($n=12$)	66.1	112.5	22.4	119.9	33.3	71.0	4.8	1003.7	−48.9
Narrow moat ($n=16$)	17.8	127.5	18.6	128.7	28.4	67.3	3.7	1006.2	−50.4
Corr. ($n=54$)		−0.36	0.36	0.30	0.43	0.30	0.32	−0.43	0.49

[a]All listed factors exhibit significant differences between two groups with the 95% confidence level by the *t* test. Also shown in the last row are the correlation coefficients of each factor for all cases.

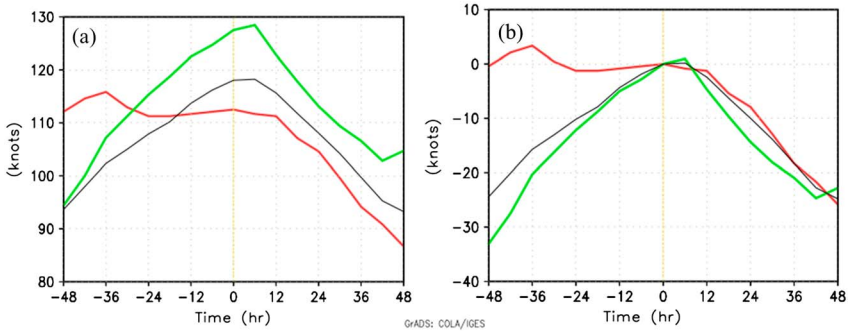

Figure 5. (a) Intensity changes before and after the detection of secondary eyewalls in TCs with a wide (red) and narrow (green) moat. The black line is the mean. (b) Same as Figure 5a except normalized by the maximum intensity.

with the increase of lead time. There exist no significant correlations with upper level RH (RHHI), low-level symmetric tangential winds (TWAC), and storm intensity (VMX) in the lead times longer than 18 h (Figure 6). Different from the weakening correlation with VMX, the correlations with MPI strengthen with increasing lead time (Figure 6).

4.3. Stepwise Regression

[29] Prior to regression, all variables are normalized by subtracting their means and dividing by their standard deviations. This allows the direct comparison of the coefficients resulting from the regression process. A stepwise regression procedure is used to select variables. The significance of each variable selected is based on a standard *F* test [*Panofsky and Brier*, 1968]. A 99% statistical significance level is required for an individual variable to be included in the model. Once in the model, a variable can only be removed if its significance level falls below 99% by the addition/removal of another variable. The stepwise procedure identifies important predictors at each time.

[30] Interestingly, RH at the upper levels (RHHI) instead of lower levels (RHLO) is included in the forecast models. The environmental factors CAPE, as well as SPD, U200, DIV200, the factors related to vertical wind shear (SHRS, USHRD, and USHRS), TWAC, and SST are not chosen at any selection step. Although significant correlations with secondary eyewall size are observed in MPI and TWAC, these two factors are not selected due to their high correlation with other predictors (Figure 6). VMX and DVMX24, instead of MPI, reflect the contributions of storm intensity to the variation of secondary eyewall size. Since high low-level relative vorticity is favorable for TC development and intensification [*Gray*, 1979; *Camargo and Sobel*, 2005; *Ventham and Wang*, 2007; *Wang and Zhou*, 2008], the contribution of ambient low-level vorticity (VOR850) to moat size is also related to storm intensity. TWAC is found highly related with T200 and PENC with mutual correlation coefficients around 0.7.

[31] The predictors chosen at each forecast time are not necessarily the same. In order to maintain continuity, the stepwise regression is reperformed, such that the predictors significant at the 99% confidence level for at least two consecutive forecast lead times in the first regression equations are selected. As a result, the seven most important predictors, namely VMX, LAT, VOR850, PENC, RHHI, T200, and DVMX24, are included in the final predictor pool. To avoid overfitting, we finally select only four predictors, less than 10% of the sample size (54) for each lead time regression. The relative contribution of each variable for each forecast lead time can be illustrated by the values associated with the normalized regression coefficient. The potential forecast capabilities of this model are estimated in terms of the variance explained (R^2). The prediction scheme is able to explain 30%–40% of the total variance of the secondary eyewall size (Table 4).

[32] It is interesting to note that the prediction of moat size also has several common factors with the empirical model which is used to predict the possibility of secondary eyewall formation in a given storm [*Kossin and Sitkowski*, 2009]. For example, the possibility of the occurrence of a secondary eyewall in the northern Atlantic is also related to the latitude of storm center and storm intensity. The possibility becomes higher for storms at lower latitude with stronger intensity, but the size of the secondary eyewall is usually small based on our result. Common factors also include surface pressure at outer edge of vortex (PENC), upper level relative humidity (RHHI), and symmetric tangential wind (TWAC). These three environmental features are favorable for secondary eyewall formation and also favorable for large-size moats.

[33] Table 4 lists the normalized coefficients associated with each forecast lead from 48 to 0 h in 6 h intervals. The predictors VMX, RHHI, and T200 are essential for short lead time forecasts but become less important and are replaced by DVMX24, LAT, VOR850, and PENC with the increase of lead time. The weakening contributions of VMX and RHHI

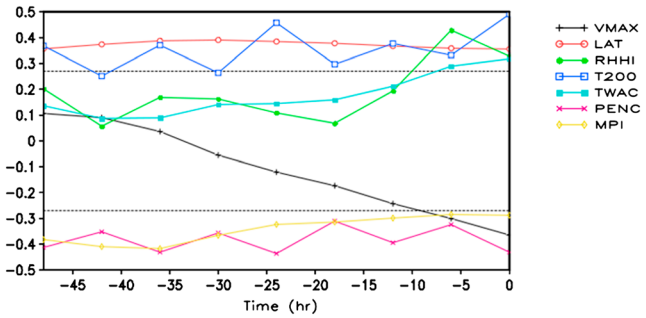

Figure 6. The correlations of secondary eyewall size with TC intensity (VMX), TC latitude, upper level RH, 200 hPa temperature (T200), low-level symmetric tangential winds (TWAC), surface pressure (PENC), and MPI. The time coordinate is referenced to the time of secondary eyewall detection. The dashed black lines mark the 95% significant level.

Table 4. A List of Normalized Regression Coefficients, Variance Explained (R^2), and F Value[a]

	1	2	3	4	5	6	7			
Hour	VMX	T200	RHHI	VOR850	PENC	LAT	DVMX24	F	R^2	SS
0	−0.27	0.49	0.22	−0.30				8.7	0.42	12.0%
−6	−0.35		0.41	−0.39	−0.41			9.0	0.42	16.5%
−12	−0.29		0.29		−0.23	0.33		6.3	0.34	7.8%
−18	−0.18				−0.21	0.26		4.0	0.29	3.5%
−24	−0.23	0.34		−0.24	−0.32			5.4	0.31	−0.5%
−30				−0.28	−0.50	0.27	−0.20	5.9	0.32	7.7%
−36				−0.28	−0.42	0.27	−0.18	7.2	0.37	7.8%
−42				−0.26	−0.50	0.28	−0.15	5.0	0.30	8.5%
−48				−0.22	−0.42	0.26	−0.17	5.9	0.32	9.8%

[a]The forecast times are listed at the left side of the table. The critical value of F at the 95% confidence level corresponding to $k-1=3$ and $n-k=50$ degrees of freedom is 2.97. SS is the forecast skill in independent testing.

are consistent with the correlation analyses. The term of VMX is replaced by DVMX24 and VOR850, and the term of PENC replaces T200, becoming a dominant predictor with the increase of forecast lead time.

[34] A jackknifing (leave-one-out) method is used to validate the prediction skill. A secondary eyewall event is withheld from the training sample, and the regression coefficients are recomputed without it. Forecasts and associated errors are produced for the secondary eyewall event. Then the process is repeated for every other secondary eyewall event. The performance of independent data is estimated by the forecast skill score (SS)

$$\mathrm{SS} = 1 - \frac{\mathrm{MSE}_{\mathrm{forecast}}}{\mathrm{MSE}_{\mathrm{ref}}}$$

MSE stands for mean squared error. SS is calculated against climatology. The linear regression model performs with useful skill except at 24 h.

5. Discussion: What Controls the Secondary Eyewall Size?

5.1. Storm Intensity and Intensity Change

[35] *Merrill* [1984] has shown that there is a weak but *positive* correlation coefficient between storm size (measured as the radius of the outermost closed isobar) and intensity using a large sample of storms for the North Atlantic and Pacific basins. It is believed that the separation of intensity and size as two important properties of TCs is physically and energetically consistent [*Holland*, 1983]. *Smith et al*. [2009] proposed that the increases of the maximum wind speed in the eyewall and storm size are governed by different mechanisms. The increase of the vortex size involves the convergence of absolute angular momentum above the boundary layer while storm intensity is related to the convergence within the boundary layer.

[36] Our result suggests that TC intensity and secondary eyewall size are *negatively* correlated. The examination of intensity change tendencies prior to secondary eyewall detection shows that secondary eyewalls form at a small radius during the rapid intensification process and the storms with wide moats tend to weaken prior to secondary eyewall formation. The storms with large secondary eyewalls are relatively weak compared with those with small secondary eyewalls at the time of formation.

[37] *Sitkowski et al*. [2011] documented typical intensity and structure changes associated with Atlantic basin eyewall replacement cycles using flight-level observations in conjunction with microwave imagery. It was found that the formation of the wind maximum in in situ data precedes detection of the outer eyewall in microwave imagery. The weakening was already well under way by the time a secondary convective ring with a well-defined moat appeared in microwave imagery.

[38] The inverse correlation between outer eyewall size and intensity is probably a result of the weakening of intensity before the recognition of an outer eyewall. However, the TC intensity data with 6 h intervals used in this study is satellite derived [*Dvorak*, 1975]. It is also possible that inverse correlation only reflects the dependence of satellite-derived intensity on TC structure.

5.2. Upper Level Relative Humidity

[39] The term of RHHI has a positive contribution, which means that a large (small) secondary eyewall forms in a relatively moist (dry) environment. This result is consistent with the effect of environmental RH on general storm size. *Hill and Lackmann* [2009] examined the dependence of TC size on environmental humidity through idealized numerical simulations of identical initial TC vortices in environments of varying relative humidity. Their results show that TCs in a dry environment were smaller by any measure than TCs in a moist environment. The coverage of precipitation occurring outside the TC core region is strongly sensitive to the environmental humidity. Increasing environmental moisture enhances the formation of outer rainbands and leads to a larger storm [*Kimball*, 2006]. Environmental humidity could affect secondary eyewall size in a very similar way, which is confirmed by a set of idealized numerical experiments. Following *Zhou and Wang*'s [2011] work, we conducted two parallel numerical experiments, in which the same model configurations and initial conditions are used except that one has a moister environment. The sensitivity numerical experiments confirm that the outer eyewall forms at a larger radius in the moist environment (not shown). This result will be documented separately in another paper.

5.3. TC's Central Latitude

[40] Numerical simulations [*Yamasaki*, 1968; *DeMaria and Pickle*, 1988] and observations [*Merrill*, 1984] show that low-latitude storms are smaller than high-latitude storms. The convergence of absolute angular momentum above the

boundary layer is responsible for the spin-up of the outer circulation (i.e., to increase of vortex size) [*Smith et al*., 2009]. As to latitude increases, there is an increase of the reservoir of planetary angular momentum for the vortex to draw upon. The tendency for the secondary eyewalls to form at large (small) radii in the storms located at high (low) latitude is consistent with the relationship between general storm size and latitude.

5.4. Sea-Level Pressure

[41] The negative contribution of PENC indicates that low environmental surface pressure is favorable for the formation of a large-size secondary eyewall. Previous studies have demonstrated that the storm size varies with environmental pressure [*Holland*, 1983; *Lander*, 1994; *Cocks and Gray*, 2002]. Analyses of environmental surface pressure showed that gyres, referred to as a distinct type of TC with very large circulations, are associated with broad areas of comparatively low pressure [*Cocks and Gray*, 2002]. The gyres usually develop from the monsoon trough as a discrete mode of TC genesis and slowly intensify while moving westward toward the coast of Southeast Asia. *Emanuel* [1986] and *Rotunno and Emanuel* [1987] investigated TC size and emphasized the size of the initial disturbance as a determining factor. The importance of initial vortex size is confirmed in an idealized numerical modeling study [*Xu and Wang*, 2010]. It is possible that the effect of environmental sea-level pressure on secondary eyewall size is related to the original storm size.

6. Summary and Further Discussion

[42] Observations show that the location of secondary eyewalls varies considerably. The separation distance between the two eyewalls ranges from less than 10 to more than 100 km. The location of a secondary eyewall affects the extent of destructive winds, heavy rainfall, and likely areas for storm surge. It also affects the subsequent eyewall replacement and associated intensity changes. These facts imply that secondary eyewall size is an important issue in TC forecasting. Many possible mechanisms for secondary eyewall formation have been proposed in the literature. It is generally suggested that the radial location of a secondary eyewall is closely related to the storm's internal dynamic or thermodynamic processes. In this study, the environmental conditions surrounding TCs with secondary eyewalls are investigated by using composite, correlation, and stepwise regression analyses.

[43] Several important factors that could affect secondary eyewall size are identified. It is found that secondary eyewall size is negatively correlated with TC intensity and environmental low-level vorticity. Large secondary eyewalls form in relatively weak storms, and the weakening starts prior to secondary eyewall formation. In contrast, small secondary eyewalls tend to form during a rapid intensification process. The results also suggest that large secondary eyewalls tend to form in high-latitude, moist, low-pressure environment.

[44] The influence of storm latitude, environmental relative humidity, and sea-level pressure on secondary eyewall size is consistent with their known influence on general storm size. These environmental factors are favorable for the formation of a large-size secondary eyewall, as well as a large-size storm. It is possible that the secondary eyewall likely forms at a larger radius in the storms with a larger horizontal extent. The storm size generally increases after the first secondary eyewall event. This is probably the reason that the secondary eyewalls in the second secondary eyewall cycle are larger than those in the first cycle. In other words, the increase of storm size could result in the larger secondary eyewall size in the second secondary eyewall event than in the first one. Western North Pacific storms are generally larger than their North Atlantic counterparts and, on average, cover twice the area [*Merrill*, 1984]. One could speculate that the size of secondary eyewalls is generally larger in the WNP than in the Atlantic.

[45] A multiple linear regression model was developed using these predictors. The linear regression model performs skillfully against climatology in independent testing. With the increase of forecast lead time, environmental sea-level pressure becomes a dominant factor affecting secondary eyewall size, whereas the contribution of environmental humidity decreases notably. At the longer lead times, significant contributions come from the environmental low-level vorticity and 24 h intensity change, instead of storm intensity.

[46] The prediction scheme is only based on TC and synoptic-environmental parameters. Explicit information about the characteristics of a TC's internal structure is missing. There is a substantial potential to improve the model in the future by including the convective characteristics, such as the areal coverage of TC-related clouds and precipitation, and the location and size of outer rainbands based on satellite observations.

[47] Although the Bayesian probabilistic model developed by *Kossin and Sitkowski* [2009] is to predict the occurrence of secondary eyewall while the regression model in this study is to predict moat size, they have some common predictors, that is, the upper level relative humidity, surface pressure, storm intensity, and central latitude. To build a complete statistical operational model, the prediction of imminent secondary eyewall formation is required. A probabilistic model similar to *Kossin and Sitkowski*'s [2009] should be developed for the WNP in the future.

[48] **Acknowledgments.** We thank H.-C. Kuo for providing the data of the secondary eyewall events over the west Northern Pacific. We also deeply appreciate the insightful comments and suggestions made by three anonymous reviewers which lead to a significantly improved manuscript. This research is supported by the NASA project (NNX09AG97G).

References

Abarca, S. F., and M. T. Montgomery (2013), Essential dynamics of secondary eyewall formation, *J. Atmos. Sci.*, doi:10.1175/JAS-D-12-0318.1, in press.

Black, M. L., and H. E. Willoughby (1992), The concentric eyewall cycle of Hurricane Gilbert, *Mon. Weather Rev.*, *120*, 947–957.

Camargo, S. J., and A. H. Sobel (2005), Western North Pacific tropical cyclone intensity and ENSO, *J. Clim.*, *18*, 2996–3006.

Cheung, K. K. W. (2004), Large-scale environmental parameters associated with tropical cyclone formations in the western North Pacific, *J. Clim.*, *17*, 466–484.

Cocks, S. B., and W. M. Gray (2002), Variability of the outer wind profiles of western North Pacific typhoons: Classifications and techniques for analysis and forecasting, *Mon. Weather Rev.*, *130*, 1989–2005.

DeMaria, M., and J. D. Pickle (1988), A simplified system of equations for simulation of tropical cyclones, *J. Atmos. Sci.*, *45*, 1542–1554.

DeMaria, M., M. Mainelli, L. K. Shay, J. A. Knaff, and J. Kaplan (2005), Further improvements to the Statistical Hurricane Intensity Prediction Scheme (SHIPS), *Weather Forecast.*, *20*, 531–543.

Dodge, P., R. W. Burpee, and F. D. Marks (1999), The kinematic structure of a hurricane with sea level pressure less than 900 mb, *Mon. Weather Rev.*, *127*, 987–1,004.

Dvorak, V. (1975), Tropical cyclone intensity analysis and forecasting from satellite imagery, *Mon. Weather Rev.*, *103*, 420–430.
Emanuel, K. A. (1986), An air-sea interaction theory for tropical cyclones: Part I: Steady state maintenance, *J. Atmos. Sci.*, *43*, 585–605.
Fang, J., and F. Zhang (2012), Effect of beta shear on simulated tropical cyclones, *Mon. Weather Rev.*, *140*, 3327–3346.
Fortner, L. E. (1958), Typhoon Sarah, 1956, *Bull. Am. Meteorol. Soc.*, *30*, 633–639.
Gray, W. M. (1979), Hurricanes: Their formation, structure and likely role in the tropical circulation. Meteorology over tropical oceans, D. B. Shaw (Ed.), Roy. Meteor. Soc., James Glaisher House, Grenville Place, Bracknell, Berkshire, RG12 1BX, 155–218.
Hawkins, J. D., M. Helveston, T. F. Lee, F. J. Turk, K. Richardson, C. Sampson, J. Kent, and R. Wade (2006), Tropical cyclone multiple eyewall configurations, *Preprints, 27th Conference on Hurricanes and Tropical Meteorology, Monterey, CA, Amer, Meteror. Soc.*
Hendricks, A. E., M. S. Peng, B. Fu, and T. Li (2010), Quantifying environmental control on tropical cyclone intensity change, *Mon. Weather Rev.*, *138*, 3243–3271.
Hill, A. K., and G. M. Lackmann (2009), Influence of environmental humidity on tropical cyclone size, *Mon. Weather Rev.*, *137*, 3294–3315.
Holland, G. J. (1983), Tropical cyclones in the Australian/southwest Pacific region, Atmos. Sci. Rep., 363, Colorado State University, Fort Collins, CO, 264 pp.
Houze, R. A., Jr. (1993), *Cloud Dynamics*, pp. 573, Academic Press, San Diego.
Houze, R. A., et al. (2006), The hurricane rainband and intensity change experiment: Observations and modeling of Hurricanes Katrina, Ophelia, and Rita, *Bull. Am. Meteorol. Soc.*, *87*, 1503–1521.
Houze, R. A., Jr., S. S. Chen, B. F. Smull, W.-C. Lee, and M. M. Bell (2007), Hurricane intensity and eyewall replacement, *Science*, *315*, 1235–1239.
Huang, Y.-H., M. T. Montgomery, and C.-C. Wu (2012), Concentric eyewall formation in Typhoon Sinlaku (2008). Part II: Axisymmetric dynamical processes, *J. Atmos. Sci.*, *69*, 662–674.
Kalnay, E., et al. (1996), The NCEP/NCAR 40-year reanalysis project, *Bull. Am. Meteorol. Soc.*, *77*, 437–471.
Kepert, J. D. (2013), How does the boundary layer contribute to eyewall replacement cycles in axisymmetric tropical cyclones?, *J. Atmos. Sci.*, doi:10.1175/JAS-D-13-046.1, in press.
Kimball, S. K. (2006), A modeling study of hurricane landfall in a dry environment, *Mon. Weather Rev.*, *134*, 1901–1918.
Knaff, J. A., C. R. Sampson, and M. DeMaria (2005), An operational statistical typhoon intensity prediction scheme for the western North Pacific, *Weather Forecast.*, *20*, 688–699.
Kossin, J. P., and M. Sitkowski (2009), An objective model for identifying secondary eyewall formation in hurricanes, *Mon. Weather Rev.*, *137*, 876–892.
Kruskal, W. H., and W. A. Wallis (1952), Use of ranks in one-criterion variance analysis, *J. Am. Stat. Assoc.*, *47*, 583–621.
Kummerow, C., W. Barnes, T. Kozu, J. Shiue, and J. Simpson (1998), The tropical rainfall measuring mission (TRMM) sensor package, *J. Atmos. Oceanic Technol.*, *15*, 809–817.
Kuo, H.-C., L.-Y. Lin, C.-P. Chang, and R. T. Williams (2004), The formation of concentric vorticity structures in typhoons, *J. Atmos. Sci.*, *61*, 2722–2734.
Kuo, H.-C., W. H. Schubert, C.-L. Tsai, and Y.-F. Kuo (2008), Vortex interactions and barotropic aspects of concentric eyewall formation, *Mon. Weather Rev.*, *136*, 5183–5198.
Kuo, H.-C., C.-P. Chang, Y.-T. Yang, and H.-J. Jiang (2009), Western North Pacific typhoons with concentric eyewalls, *Mon. Weather Rev.*, *137*, 3758–3770.
Lander, M. A. (1994), Description of a monsoon gyre and its effects on the tropical cyclones in the western North Pacific during August 1991, *Weather Forecast.*, *9*, 640–654.
Maclay, K. S., M. DeMaria, and T. H. Vonder Haar (2008), Tropical cyclone inner-core kinetic energy evolution, *Mon. Weather Rev.*, *136*, 4882–4898.
Merrill, R. T. (1984), A comparison of large and small tropical cyclones, *Mon. Wea. Rev.*, *112*, 1408–1418.
Montgomery, M. T., and R. J. Kallenbach (1997), A theory for vortex Rossby waves and its application to spiral bands and intensity changes in hurricanes, *Q. J. R. Meteorol. Soc.*, *123*, 435–465.
Nong, S., and K. Emanuel (2003), A numerical study of the genesis of concentric eyewalls in hurricanes, *Q. J. R. Meteorol. Soc.*, *129*, 3323–3338.
Panofsky, H. A., and G. W. Brier (1968), *Some applications of statistics to meteorology*, 224 pp., Earth and Mineral Sciences Continuing Education, College of Earth and Mineral Sciences, The Pennsylvania State University, University Park, PA, USA.
Rotunno, R., and K. A. Emanuel (1987), An air-sea interaction theory for tropical cyclones. Part II: Evolutionary study using a nonhydrostatic axisymmetric numerical model, *J. Atmos. Sci.*, *44*, 542–561.
Rozoff, C. M., W. H. Schubert, B. D. McNoldy, and J. P. Kossin (2006), Rapid flamentation zones in intense tropical cyclones, *J. Atmos. Sci.*, *63*, 325–340.
Rozoff, C. M., D. S. Nolan, J. P. Kossin, F. Zhang, and J. Fang (2012), The roles of an expanding wind field and inertial stability in tropical cyclone secondary eyewall formation, *J. Atmos. Sci.*, *69*, 2621–2643.
Samsury, C. E., and E. J. Zipser (1995), Secondary wind maxima in hurricanes: Airflow and relationship to rainbands, *Mon. Weather Rev.*, *123*, 3502–3517.
Shapiro, S. S., and M. B. Wilk (1965), An analysis of variance test for normality (complete samples), *Biometrika*, *52*(3–4), 591–611.
Shapiro, L. J., and H. E. Willoughby (1982), The response of balanced hurricanes to local sources of heat and momentum, *J. Atmos. Sci.*, *39*, 378–394.
Sitkowski, M., J. P. Kossin, and C. M. Rozoff (2011), Intensity and structure changes during hurricane eyewall replacement cycles, *Mon. Weather Rev.*, *139*, 3829–3847.
Smith, R. K., M. T. Montgomery, and N. V. Sang (2009), Tropical cyclone spin-up revisited, *Q. J. R. Meteorol. Soc.*, *135*, 1321–1335.
Terwey, W. D., and M. T. Montgomery (2008), Secondary eyewall formation in two idealized, full-physics modeled hurricanes, *J. Geophys. Res.*, *113*, D12112, doi:10.1029/2007JD00897.
Trenberth, K. E., and C. J. Guillemot (1998), Evaluation of the atmospheric moisture and hydrological cycle in the NCEP/NCAR reanalyses, *Clim. Dyn*, 213–231, doi:10.1007/s003820050219.
Ventham, J. D., and B. Wang (2007), Large scale flow patterns and their influence on the intensification rates of western North Pacific tropical storms, *Mon. Weather Rev.*, *135*, 1110–1127.
Wang, B., and X. Zhou (2008), Climate variation and prediction of rapid intensification in tropical cyclones in the western North Pacific, *Meteorol. Atmos. Phys.*, *99*, 1–16.
Wang, X., Y. Ma, and N. E. Davidson (2013), Secondary eyewall formation and eyewall replacement cycles in a simulated hurricane: Effect of the net radial force in the hurricane boundary layer, *J. Atmos. Sci.*, *70*, 1317–1341.
Weatherford, C. L., and W. M. Gray (1988a), Typhoon structure as revealed by aircraft reconnaissance. Part I: Data analysis and climatology, *Mon. Weather Rev.*, *116*, 1032–1043.
Weatherford, C. L., and W. M. Gray (1988b), Typhoon structure as revealed by aircraft reconnaissance. Part II: Structural variability, *Mon. Weather Rev.*, *116*, 1044–1056.
Willoughby, H. E. (1990), Gradient balance in tropical cyclones, *J. Atmos. Sci.*, *47*, 265–274.
Willoughby, H. E., and M. E. Rahn (2004), Parametric representation of the primary hurricane vortex. Part I: Observations and evaluation of the Holland (1980) model, *Mon. Weather Rev.*, *132*, 3033–3048.
Willoughby, H. E., J. A. Clos, and M. G. Shoreibah (1982), Concentric eyewalls, secondary wind maxima, and the evolution of the hurricane vortex, *J. Atmos. Sci.*, *39*, 395–411.
Willoughby, H. E., H.-L. Jin, S. J. Lord, and J. M. Piotrowicz (1984), Hurricane structure and evolution as simulated by an axisymmetric, nonhydrostatic numerical model, *J. Atmos. Sci.*, *41*, 1169–1186.
Xu, J., and Y. Wang (2010), Sensitivity of the simulated tropical cyclone inner-core size to the initial vortex size, *Mon. Weather Rev.*, *138*, 4135–4157.
Yamasaki, M. (1968), Numerical simulation of tropical cyclone development with the use of the primitive equations, *J. Meteorol. Soc. Jpn*, *46*, 202–214.
Zhou, X., and B. Wang (2011), Mechanism of concentric eyewall replacement cycles and associated intensity change, *J. Atmos. Sci.*, *68*, 972–988.